

BUCKLING AND POSTBUCKLING OF A LARGE DELAMINATED PLATE SUBJECTED TO SHEAR LOADING

Vít Obdržálek*, Jan Vrbka*

Buckling and postbuckling behaviour of a delaminated plate subjected to shear loading has been studied by means of the finite element analysis. The plate was assumed to contain either one or two circular delaminations of various diameters and of various out-of-plane and in-plane positions. The size of the plate corresponded to the size of laminate panels used in aircraft structures. It was therefore possible to assess the practical applicability of numerous studies which focused on the buckling behaviour of substantially smaller plates.

Keywords: fibre-metal laminate, plates, buckling, delamination, finite element analysis

1. Introduction

In the past 30 years, the issue of buckling and postbuckling of delaminated plates has attracted much attention due to the significant effect of delaminations upon the load carrying capacity of the laminate structures. It was shown how the size and the shape of delaminations can affect the buckling load and also how delaminations can behave in the postbuckling regime [1]. However, majority of the studies into the buckling of delaminated plates focused on the behaviour of plates with relatively small in-plane dimensions. Such plates exhibit mostly half wave (U-shaped) buckled forms or less frequently single wave (S-shaped) buckled forms with more or less significant local buckling of the delaminated sublaminates [2]. On the other hand, the laminate panels used in aircraft structures are slender enough to exhibit multiple wave buckled forms. Also the ratio of the slenderness of delaminated sublaminates with respect to the slenderness of the whole panels is different and the panels could be expected to buckle without local buckling of the delaminated sublaminates. As a result, the growth of delaminations in the postbuckling regime could be significantly altered as well. Partly because of the reduced importance of the opening fracture mode and partly because of the variable position of delamination with respect to the nodal and anti-nodal lines.

Hence, the aim of this study was to investigate the buckling and postbuckling behaviour of delaminated plates with dimensions similar to dimensions of laminate panels used in aircraft structures. In order to reflect the loading of laminate panels in aircraft structures, the plate was assumed to be subjected to shear loading. The study focused on the effects of delamination size, in-plane and out-of-plane position of delaminations upon the load carrying capacity of the plates. Two possible load limiting events were considered – buckling and delamination growth initiation.

* Ing. V. Obdržálek, prof. RNDr. Ing. J. Vrbka, DrSc., Brno University of Technology, Faculty of Mechanical Engineering, Technická 2, 616 69 Brno, Czech Republic

2. Analysis

2.1. Problem description

The buckling and postbuckling behaviour of a delaminated plate subjected to shear loading was studied. The plate was assumed to be made of fibre-metal laminate which consists of three aluminium sheets interleaved with carbon fibre/epoxy composite plies. The structure of the laminate is described in Table 1. Three sets of analyses with different out-of-plane positions of either one or two circular delaminations were performed. The first set comprised of analyses of plates with a delamination at the near surface interface A (see Table 1), the second set included plates with a delamination at the near mid-surface interface C and the last set of analyses focused on behaviour of plates with two delaminations at interfaces A and B. The first two sets were designed so in order to study behaviour of plates with two extreme positions of a single delamination, the last set of analyses focused on the effect of multiple delaminations upon the buckling load. The positions of delaminations were chosen so to obtain two neighbouring slender sublaminates and thereby to achieve maximum buckling load reduction. Plates with a greater number of delaminations were not analysed since this would have required extremely long computational times.

Layer	thickness [mm]	ply angle	interface
aluminium	0.4		A
composite	0.1575	θ	B
composite	0.1575	$-\theta$	C
aluminium	0.4		D
composite	0.1575	$-\theta$	E
composite	0.1575	θ	F
aluminium	0.4		

Tab.1: Structure of the laminate

Each set of analyses comprised of 36 analyses of a plate with a unique combination of the in-plane position of delamination(s) (four variants – see Figure 1), composite ply orientation (three variants: $\theta = 0^\circ, 45^\circ, 90^\circ$) and delamination diameter (three variants: $d = 10, 20, 40$ mm). When the plate contained two delaminations, these had always the same in-plane position and radius.

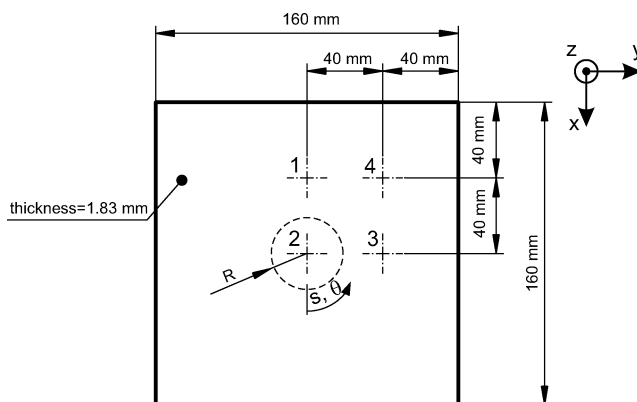


Fig.1: Plate dimensions and positions of delaminations

2.2. Finite element mesh

The plate was modelled with 8-node layered continuum shell elements (entitled SC8R in ABAQUS) which employ the first-order shear deformation theory kinematics [3]. The mesh consisted of two separate parts which represented the delaminated and nondelaminated portion of the plate. The delaminated part, consisted only of two or three layers of elements depending on the number of delaminations. Consequently, the accuracy of distributions of the components of the total energy release rate could be expected to be slightly inaccurate [1]. The nondelaminated part was modelled with just one layer of elements. The two parts of the plate were bonded by TIE constraint implemented in ABAQUS. Because the virtual crack closure technique [4, 5] was used to determine the energy release rate along the delamination boundary, the edges of elements adjacent to the boundary were made to be orthogonal in order to simplify evaluation of the results. A sample element mesh is depicted in Figure 2.

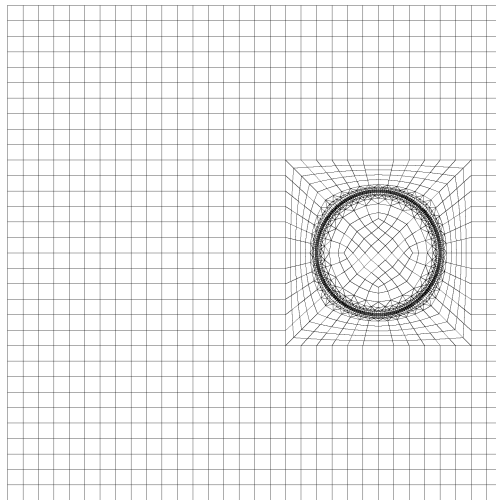


Fig.2: Sample finite element mesh

2.3. Material

Both the metal and the composite were assumed to be linear elastic. The aluminium layers were assumed to be isotropic with the Young's modulus of 0.725 GPa and Poisson's ratio of 0.34. The composite layers were modelled as orthotropic – corresponding material properties are listed in Table 2.

Hexcel unidirectional carbon/epoxy prepreg		
$E_{11} = 126.0$ GPa	$E_{22} = 11.0$ GPa	$E_{33} = 11.0$ GPa
$\nu_{12} = 0.28$	$\nu_{13} = 0.28$	$\nu_{23} = 0.40$
$G_{12} = 6.60$ GPa	$G_{13} = 6.60$ GPa	$G_{23} = 3.93$ GPa

Tab.2: Material properties of composite plies [6]

2.4. Contact constraints

To prevent unrealistic overlapping of delaminated sublaminates, a surface based frictionless contact interaction was used in between the delaminated sublaminates. The augmented Lagrangian contact algorithm was employed.

In order to ensure buckling of the initially flat plate, it was necessary to introduce an imperfection into the model. This was accomplished by introduction of a small virtual interference between the delaminated sublaminates in the delaminated region. The interference magnitude was chosen to be 1.10^{-6} m, which is less than 1% of the composite ply thickness. This value was found to be sufficiently small not to significantly affect the postbuckling response. Similar result was presented by Tay et al. [7].

2.5. Boundary conditions

The loading conditions roughly corresponded to the conditions of the experiment carried out by Featherson and Watson [8] – see Figure 3. Two opposite edges were assumed to be bonded to the rigid blocks, one of which was fixed and the other one had prescribed displacement in the edge direction (y -axis) while being allowed to translate towards the opposite edge. The other two edges were constrained to remain straight and the out-of-plane movement was not allowed.

Since the three-dimensional continuum shell elements were used to built up the plate, some arrangements had to be made in order to simulate the plate boundary conditions appropriately. Therefore, an extra set of nodes was modelled along the plate edges at the mid-surface of the plate and the movement of the nodes on the top, bottom and mid surfaces was constrained by a set of linear equations

$$u_i^{\text{top}} + u_i^{\text{bottom}} - 2u_i^{\text{mid}} = 0, \quad (1)$$

where u_i^{top} , u_i^{bottom} and u_i^{mid} are the displacements of the nodes on the top, bottom and mid surface measured along the i -direction. All the displacements corresponding to the desired in-plane movement of the plate were then prescribed at the nodes lying in the mid-plane.

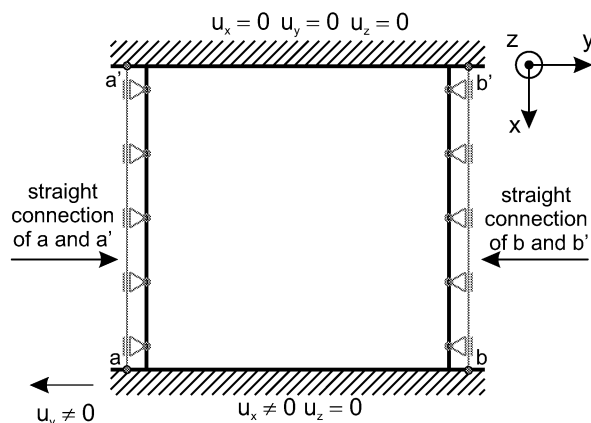


Fig.3: Mid-plane boundary conditions

2.6. Solution method

Common quasi-static nonlinear analyses were performed using Newton-Raphson method. In order to prevent divergence due to buckling of the plate, an artificial damping algorithm implemented in Abaqus was used.

3. Results

Two possible load limiting states were chosen for the evaluation of the effect of plate and delamination parameters upon the load carrying capacity of delaminated plates. The first load limiting event is the initial buckling of the plate. The second one is delamination growth initiation.

3.1. Initial buckling

The most important characteristic of the initial buckling response is the buckling load. In the present study, the buckling load was defined as a load at which the deflection of the centre of plate or the centre of a delaminated sublaminates reached $20 \mu\text{m}$. This approach was chosen to simplify evaluation of the buckling loads and provided good match with buckling loads identified by the well known Southwell plot technique [9] and by the standard linear buckling analysis.

The summary of the buckling loads is presented in Figures 4, 5 and 6. Even at the first sight it is evident, that the effect of the size of delamination was negligible in case of delaminations with diameters of 10 and 20 mm. When the delamination diameter was 40 mm, the buckling loads were usually slightly smaller. Only in the case of the plates with two large delaminations and the ply angle 45° was the reduction significant – see Figure 6. It seems that only presence of multiple large delaminations may affect the buckling load when behaviour of large plates is under consideration. This is not surprising because in case of delaminations with diameters of 10 and 20 mm, the ratio of the delamination diameter vs. the width of the plate is 0.0625 and 0.125, respectively, which values usually correspond to no or small buckling load reduction [10]. Since in reality the largest dimension of impact induced delaminations is usually not much greater than 40 mm [11–15], the initial buckling load is not likely to be significantly reduced.

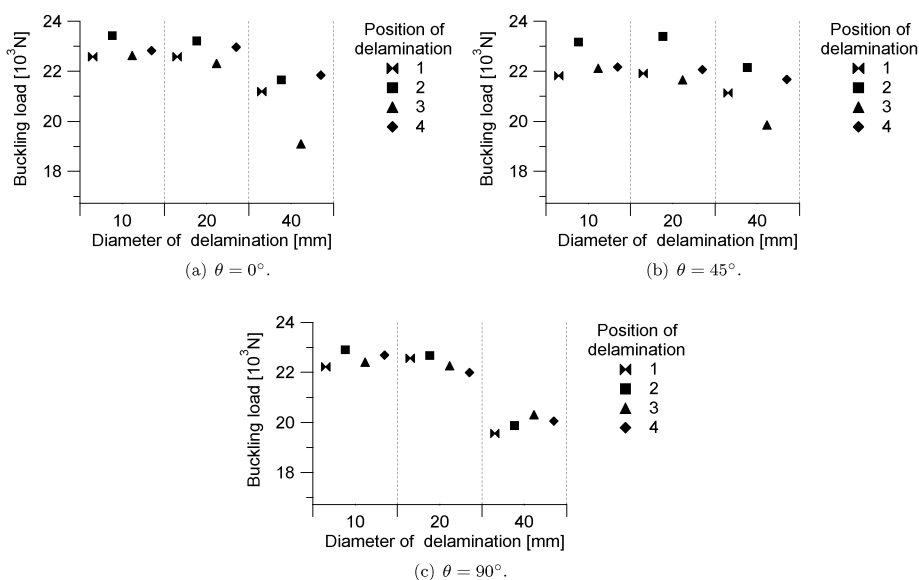


Fig.4: Buckling limit loads of plates with a circular delamination at interface A

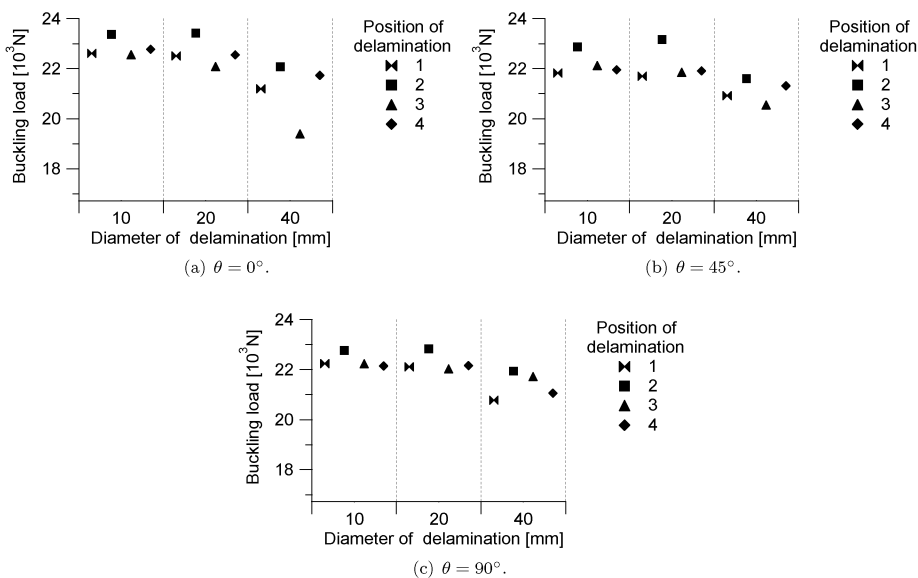


Fig.5: Buckling loads of plates with a circular delamination at interface C

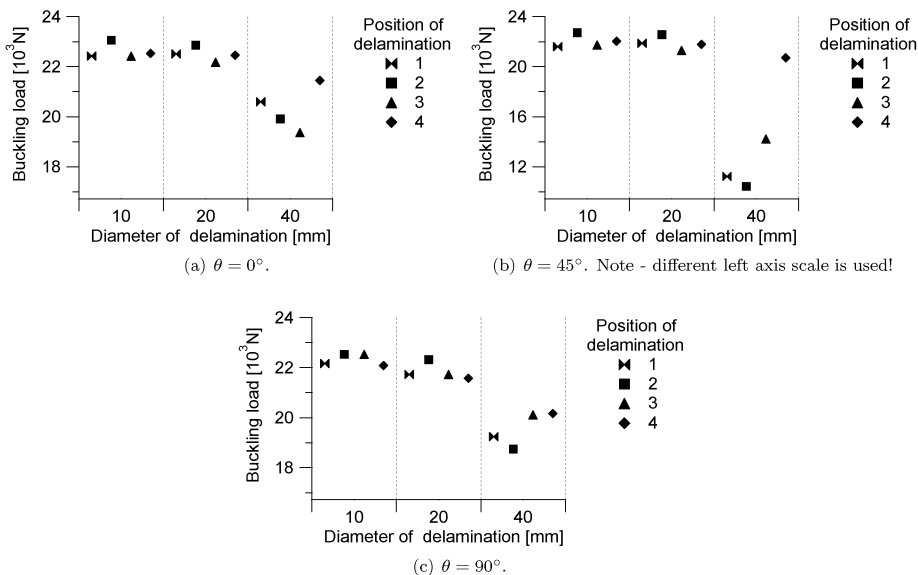


Fig.6: Buckling loads of plates with two circular delaminations positioned at interfaces A and B

The effect of the out-of-plane position of delamination upon the buckling load could be seen in Figures 4 and 5. Since small delaminations did not alter the buckling load, the effect could be observed only in case of the plates with a delamination which has the diameter of 40 mm. Such plates exhibited greater buckling loads when the delamination was near the mid-plane than when it was near the surface.

Considering the effect of the in-plane position of delamination upon the buckling load, it must be concluded that no clear effect could be observed, although it might appear that there

was some trend in case of plates with delaminations which have a diameter of 10 or 20 mm. However, the regular fluctuations of the buckling load observed in Figures 4–6 was caused by combination of several phenomena. Firstly, the different deflection rate at different regions of the plate was responsible for the fact that the maximum deflection of $20\ \mu\text{m}$ used to identify the buckling load corresponded to slightly different load levels. Secondly, the viscous damping used to avoid divergence of the computational analyses sometimes altered slightly the buckling load. And at last, the initial buckling behaviour was found to be a-priori sensitive to imperfections. This happens, when there are two or more close equilibrium load paths in the vicinity of the initial buckling point. The load-deflection curves shown in Figure 7 clearly demonstrate that the buckling mode often changed into the secondary buckling mode as the load slightly increased. It should be mentioned, that sometimes the initial buckling behaviour was so complex that no clear buckling mode could be identified. The initial buckling behaviour was not only interesting because of the identification of the buckling load but also because of the evolution of the buckled shape is crucial for the ultimate load bearing capability of the plates. Therefore, typical load-deflection curves are presented in Figures 7–9. Firstly, it should be noticed that the direction of the plate deflection varied, which could have an enormous effect upon the growth of delaminations (e.g. Figures 7(a) and 7(d)), since the delaminated sublaminate which is closer to the more compressed side may buckle locally.

The second interesting phenomenon is the evolution of the gap in between delaminated sublaminate. It is because such gap usually gives rise to the possibility of the fracture mode I driven growth of delamination. Quite often, there was no apparent gap in between delami-

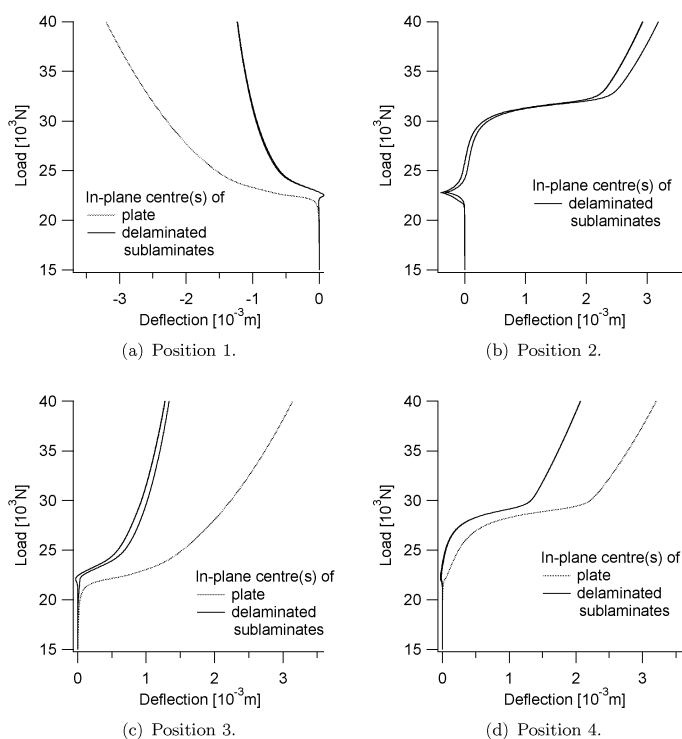


Fig. 7: Load-deflection curves – plates with a delamination at interface A, the diameter of delamination $d = 40\ \text{mm}$, the ply angle $\theta = 0^\circ$

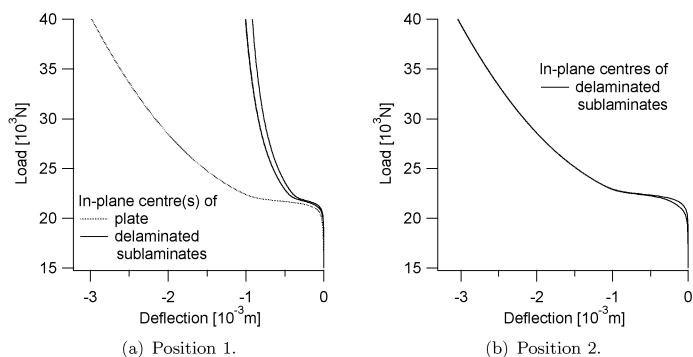


Fig.8: Load-deflection curves – plates with a delamination at interface A, the diameter of delamination $d = 40$ mm, the ply angle $\theta = 90^\circ$

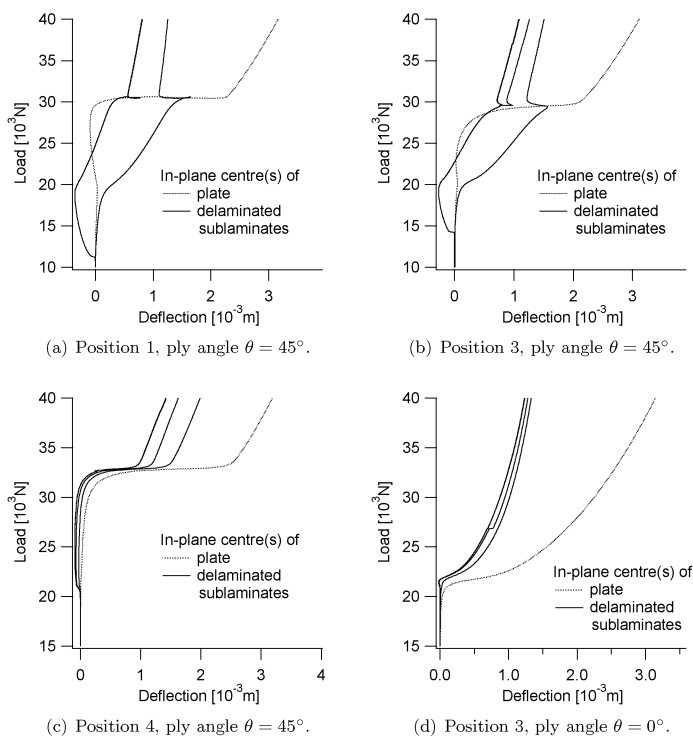


Fig.9: Load-deflection curves – plates with delaminations at interfaces A and B, the diameter of delaminations $d = 40$ mm

nated sublaminates at all (Figures 7(a) and 7(d)). This held for all plates with delaminations which had diameter of either 10 mm or 20 mm. However, in case of plates with large delaminations, the gap was usually observed at least at some load level. Sometimes, the gap was observed ever since the initial buckling, although the gap size may have varied (Figures 7(b) and 7(c)). Sometimes, the gap occurred only at higher load levels (Figure 8(a)) or on the other hand, there was the gap only in the initial stage of loading (Figure 8(b)). It should be also mentioned, that the gradual change of the buckling shape from the initial form to

the final form was sometimes accompanied by development of a huge gap in between delaminated sublaminates (the gap being positioned closer to the edge of the delamination) – see Figure 10. Such behaviour is not typical for small delaminated plates, because small plates with a large delamination, which is essential for this sort of behaviour, do not tend to change the initial buckling mode shape. In case of plates with two delaminations the situation was even more complicated because a gap in between any of the three sublaminates could occur – see Figure 9. It might be concluded, that the prediction of the buckling and postbuckling behaviour of large delaminated plates, especially when the growth of delaminations is to be predicted, could be quite difficult task.

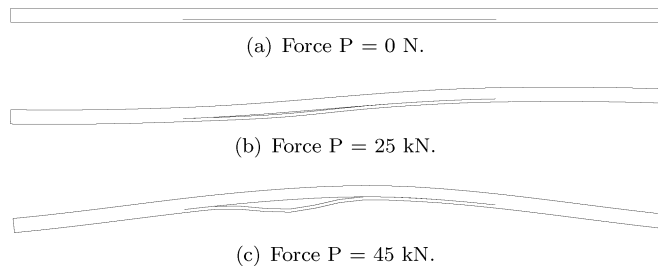


Fig.10: Gap evolution – diagonal cross-section of the 80×80 mm central region; a plate with a delamination in the in-plane centre at interface A, the diameter of delamination $d = 40$ mm, the ply angle $\theta = 0^\circ$

3.2. Delamination growth initiation

The possibility of delamination growth initiation can be demonstrated on the summary of the maximum values of the total energy release rate, $\mathcal{G}_{T,\max}$, found along the delamination boundary – see Figures 11 and 12. The values of $\mathcal{G}_{T,\max}$ are presented for all the analysed plate configurations with a single delamination and two load levels of 25 kN and 40 kN. The load of 40 kN corresponds to the moment when plates of all configuration exhibited the same three-half-wave buckled pattern (see Figure 13) and therefore the effects of various parameters, such as the delamination size or position of delamination, could be studied. The load level of 25 kN was chosen to demonstrate the possibility of delamination growth initiation at the load which is not much higher than the buckling load of a sound plate and thereby to assess the possibility of delamination growth initiation under conditions which reflect the fact that many aircraft structures are designed to take advantage of the load-carrying capacity of buckled plates.

Looking first at Figure 11 which presents values of $\mathcal{G}_{T,\max}$ at the load level of 25 kN, it can be seen, that delamination growth initiation at this load stage was unlikely because the critical value of the total energy release rate is usually greater than 120 J.m^{-2} [16–18]. On the other hand, from the summary of values of $\mathcal{G}_{T,\max}$ at the load level of 40 kN (Figure 12), it is evident, that some plates with a large delamination might experience delamination growth initiation. Some of the values of $\mathcal{G}_{T,\max}$ in Figure 12(c) are quite large and therefore delamination grow initiation might occur even at a lower load level. Nevertheless, it should also be realised, that the applied load of 40 kN is approximately twice as large as the buckling load. Since aircraft structures are not usually designed to withstand a load so much higher than the buckling load, it can be assumed, that delamination growth initiation may not be the critical load limiting event.

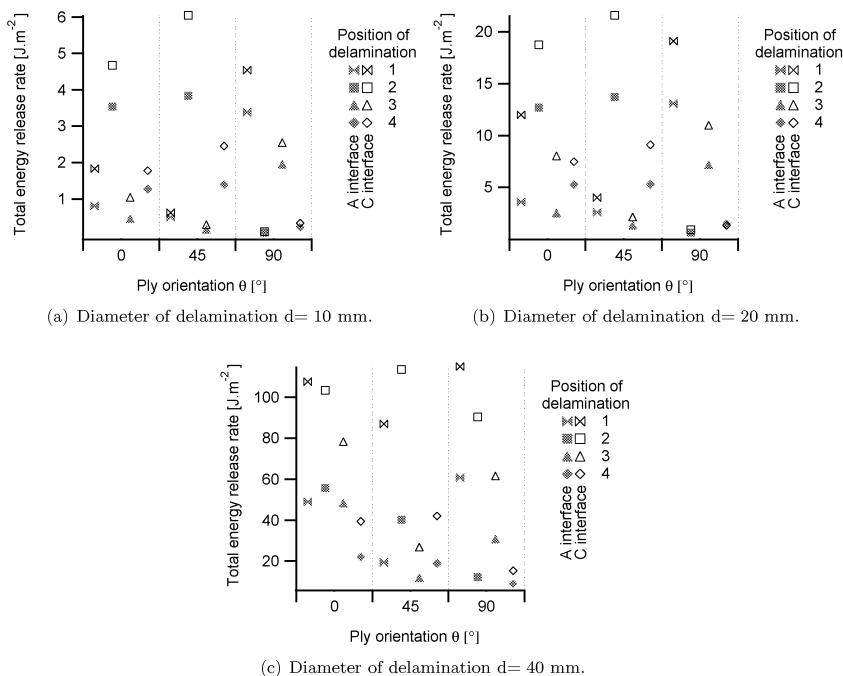


Fig.11: Maxima of the total energy release rate \mathcal{G}_T ; load $P = 25$ kN

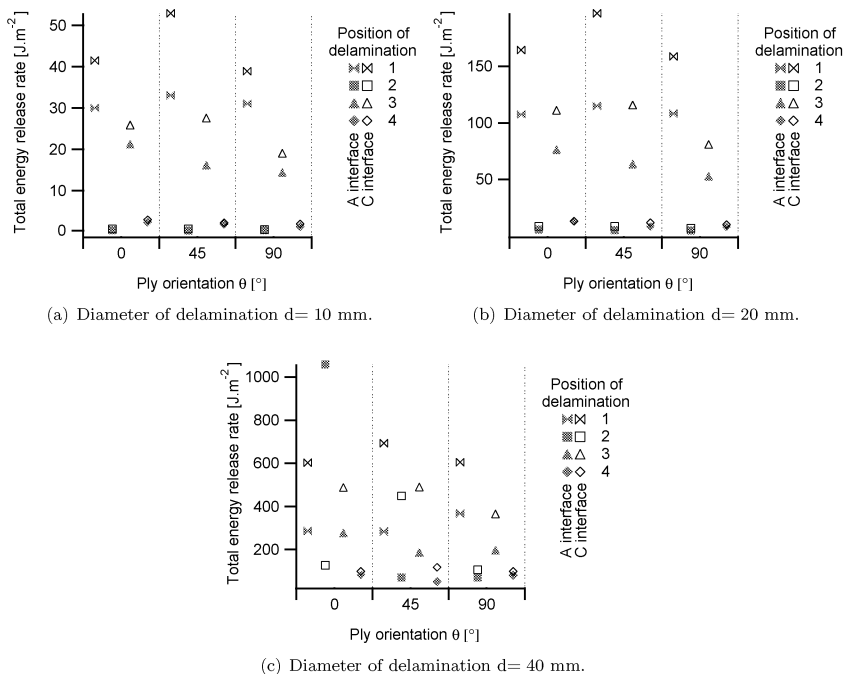


Fig.12: Maxima of total energy release rate \mathcal{G}_T ; load $P = 40$ kN

Considering the effect of the out-of-plane position of delamination upon the values of $\mathcal{G}_{T,max}$, it can be seen in both Figures 11 and 12 that, except for one case (Figure 12(c)), plates with a delamination close to the mid-plane exhibited larger $\mathcal{G}_{T,max}$ values than plates

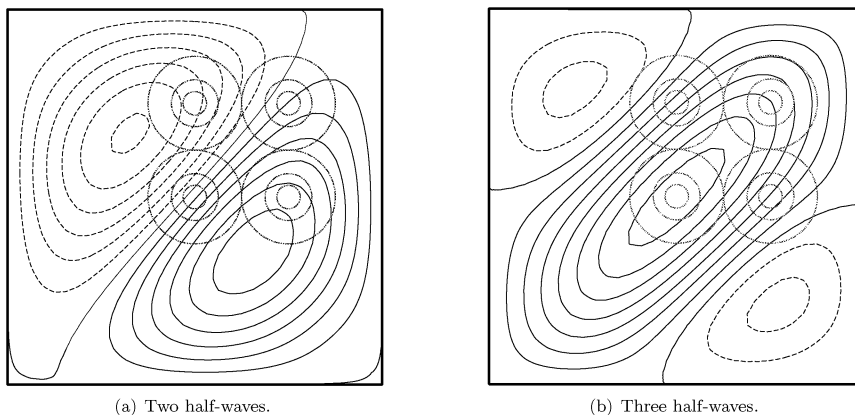


Fig.13: Buckled shapes, in-plane positions and sizes of delaminations

with a delamination near the surface. However, this does not necessarily mean that delaminations near the mid-plane would start to grow earlier than delaminations near the mid-surface, because of the dependence of the interlaminar fracture toughness upon the mode-mixity ratio.

Focusing now on the effect of the in-plane position of delaminations upon the possibility of delamination growth initiation, it can be seen in Figure 12 that plates with delaminations at position 1 or 3 (see Figure 1) exhibited larger values of $\mathcal{G}_{T,\max}$ than delaminations at position 2 or 4. Looking at Figure 13(b), it can be seen that positions 1 and 3 lie in the region with a high gradient of the out-of-plane displacement. Similarly, when two-half-wave buckling pattern, shown in Figure 13(a), was sometimes established in earlier loading stages, delaminations lying along the diagonal exhibited higher values of $\mathcal{G}_{T,\max}$ than delaminations lying off the diagonal. This feature is interesting, although possibly not generally valid. Nevertheless, it could be suggested to carry out buckling tests of the laminated structures with delaminations positioned along nodal lines of the structures because this would provide conservative values of the load-carrying capacity.

So far only the values of $\mathcal{G}_{T,\max}$ were considered. However, as it has been already mentioned, the value of the interlaminar fracture toughness could depend on the mode-mixity ratio. It is well known, that the mode II interlaminar fracture toughness is usually at least twice as large as the mode I interlaminar fracture toughness [18–22] and that there is also difference in between mode II and mode III interlaminar fracture toughnesses [23]. Therefore, information about $\mathcal{G}_{T,\max}$ might not be sufficient for delamination growth prediction. In order to get an idea about the values of the fracture mode components of \mathcal{G}_T , the summary of the maxima of all the fracture mode components at the load level 40 kN is presented in Figures 14 and 15. In Figure 14, which presents values observed in the case of plates with a delamination at interface A, it can be seen, that the maximum values of the mode I component of \mathcal{G}_T sometimes reached 38% of $\mathcal{G}_{T,\max}$ values. This means, that delaminations might start to grow in the region where \mathcal{G}_I is high rather than in the region with maximum of \mathcal{G}_T . Similarly, as it can be seen in Figures 14 and 15, the mode III component was sometimes larger than the mode II component, but again this does not mean that the location of delamination growth initiation would take place at the location where \mathcal{G}_{III} had the largest value. It is evident, that determination of values of fracture mode components of the energy release rate could be crucial for the assessment of growth of delaminations.

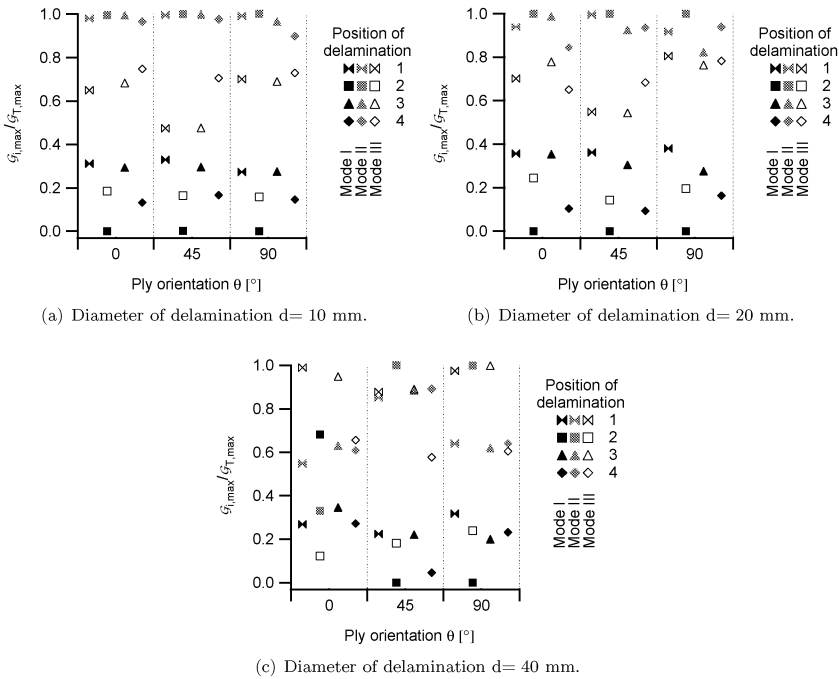


Fig.14: Maxima of the mode components of the total energy release rate \mathcal{G}_T ; load $P = 40$ kN; delamination at interface A

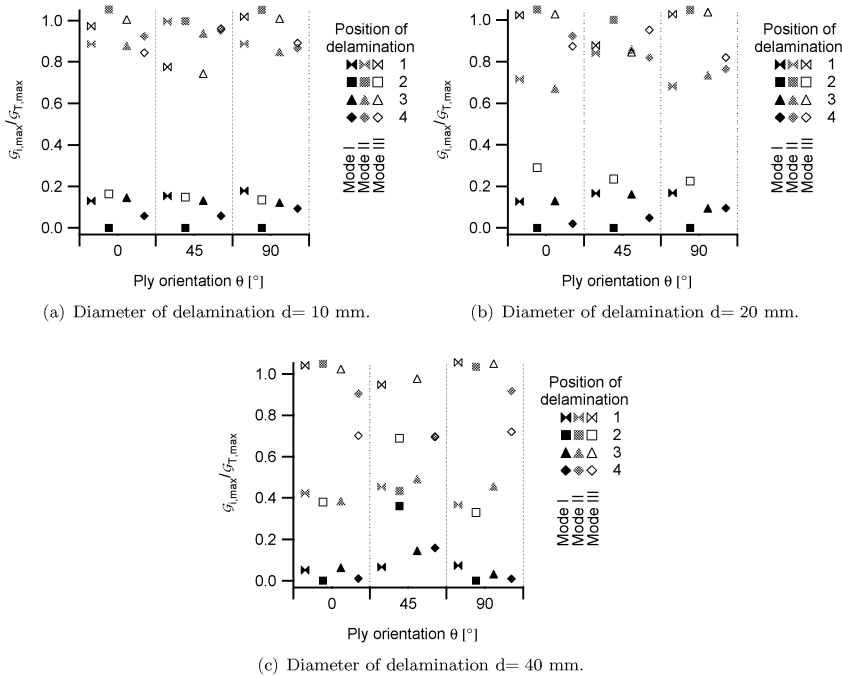
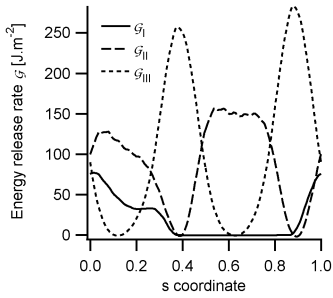


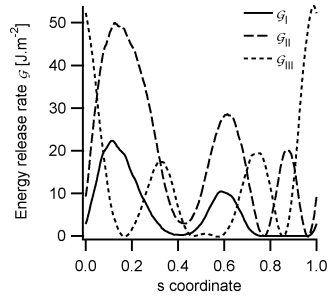
Fig.15: Maxima of the mode components of the total energy release rate \mathcal{G}_T ; load $P = 40$ kN; delamination at interface C

It should be mentioned that in case of small plates, the dominant fracture mode is usually the opening mode together with the shearing mode [7, 24, 25], and therefore the behaviour of delaminations in large and small plates is expected to be different.

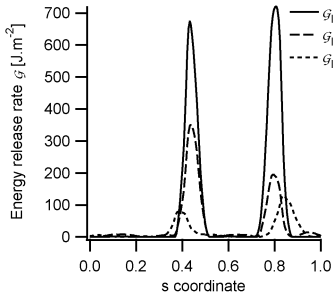
It can be also noticed, that there was some dependence of the energy release rate values upon the in-plane position of delamination. Typically, when a delamination was positioned in the centre of the plate, the only significant component of \mathcal{G}_T was the mode II component. There was, however, one exception to this rule. In the case of the plate with the ply angle $\theta = 0^\circ$ and with the large delamination positioned at interface A, the mixed buckling mode shape developed in the late loading stage, giving rise to the mode I component of the total



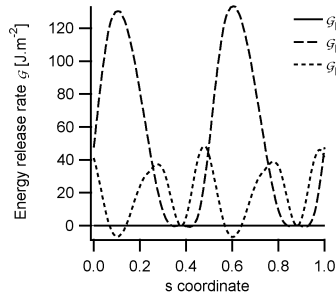
(a) Diameter of delamination $d = 40$ mm, inplane position 1, interface A, ply angle $\theta = 0^\circ$



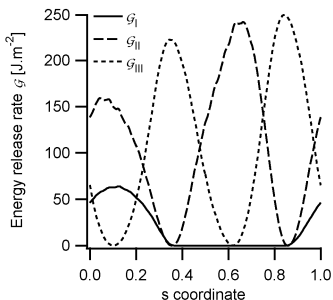
(b) Diameter of delamination $d = 40$ mm, inplane position 4, interface A, ply angle $\theta = 0^\circ$



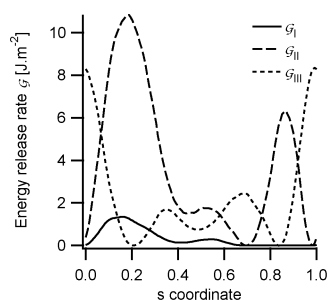
(c) Diameter of delamination $d = 40$ mm, inplane position 2, interface A, ply angle $\theta = 0^\circ$



(d) Diameter of delamination $d = 40$ mm, inplane position 2, interface C, ply angle $\theta = 0^\circ$



(e) Diameter of delamination $d = 40$ mm, inplane position 1, interface A, ply angle $\theta = 45^\circ$



(f) Diameter of delamination $d = 20$ mm, inplane position 4, interface A, ply angle $\theta = 0^\circ$

Fig.16: Typical distributions of the fracture mode components of the total energy release rate \mathcal{G}_T ; load $P = 40$ kN; plates with a single delamination; coordinate s has zero value at the bottom of a delamination and increases with counterclockwise movement along the delamination boundary as shown in Figure 1

energy release rate. In case of the other delamination positions, there was quite a resemblance in the ratio of the fracture mode components of \mathcal{G}_T . The values corresponding to delaminations at position 1 and 3 exhibited a better match compared to delaminations at position 4, since as already discussed, regions near position 1 and 3 exhibit similar deformation. There is also one more thing interesting about delaminations at position 4. In every but this position, the mode III energy release rate became more significant as the size of a delamination increased. This could be possibly attributed to the specific deformation in this region and also to the effect of boundary conditions.

A careful examination of the Figure 15 reveals that some values are greater than 1. The reason for this is that sometimes the values of the fracture mode components of the total energy release rate were negative at some places along the delamination boundary – see Figure 16(d). The occurrence of the negative values is believed to be caused by the coarse finite element mesh, since in the case of small plates which were discretised with greater number of layers of elements no negative values were observed [1].

Typical distributions of the energy release rates are presented in Figure 16. It can be seen, the mode II and mode III components of the total energy release rate are usually greater than the mode I component. Moreover, it is evident, that the ratio of the components of \mathcal{G}_T varies greatly along the delamination boundary as well as from one plate configuration to another. Therefore, if the delamination growth initiation is to be predicted, it is necessary to have information about the mixed-mode interlaminar fracture toughness value vs. the mode mixity ratio. It should be also noticed, that the interlaminar fracture toughness is a function of the orientation of plies adjacent to the delaminated interface [26, 27], which fact further complicates possibility of finding a simple procedure for prediction of the growth of delaminations in buckled delaminated composite structures.

4. Conclusions

The results of the present study can be summarised as follows:

- The effect of the size of a delamination upon the buckling load was small except for the case of plates with two delaminations with a diameter of 40 mm.
- Plates with a delamination near to the mid-surface exhibited higher values of the maximum of the total energy release rate found at the delamination boundary than plates with a near surface delamination.
- Buckled plates with a delamination lying near a nodal line exhibited higher values of the maximum total energy release rate found at the delamination boundary than plates with a delamination near an anti-nodal line. The mode-mixity was function of the in-plane position of delamination as well.
- A delamination in a large plate can start to grow only at a load which is much higher than the buckling load.
- The maximum values of the mode II and/or mode III components of the total energy release rate were found to be greater than the mode I component values in case of nearly all analysed variants of delaminated plates.
- The knowledge of the dependence of the interlaminar fracture toughness upon the mode-mixity ratio and the mutual orientation of plies adjacent to the delaminated interface is essential for accurate prediction of delamination growth.

References

- [1] Obdržálek V.: Buckling and postbuckling of delaminated plates, Ph.D. thesis, Brno University of Technology (to appear)
- [2] Lee J., Gürdal Z., Griffin O.H.: Layer-wise approach for the bifurcation problem in laminated composites with delaminations, *AIAA Journal* 31 (1993), p. 331
- [3] Reddy J.N.: *Mechanics of laminated composite plates and shells: theory and analysis*, 2nd edition, CRC Press 2004
- [4] Rybicki E.F., Kanninen M.F.: A finite element calculation of stress intensity factors by a modified crack closure integral, *Engineering Fracture Mechanics* 9 (1977), p. 931
- [5] Krueger R.: The virtual crack closure technique: history, approach and applications, Tech. rep. NASA/CR-2002-211628, NASA Langley Research Center, April 2002
- [6] Soden P.D., Hinton M.J., Kaddour A.S.: Lamina properties, lay-up and loading conditions for a range of fibre-reinforced composite laminates, *Composites Science and Technology* 58 (1998), p. 1011
- [7] Tay T.E., Shen F., Lee K.H., Scaglione A., Sciuva M.D.: Mesh design in finite element analysis of post-buckled delamination in composite laminates, *Composite Structures* 47 (1999), p. 603
- [8] Featherson C.A., Watson A.: Buckling of optimised flat composite plates under shear and in-plane bending. *Composite Science and Technology* 65 (2005), p. 839
- [9] Southwell R.V.: On the analysis of experimental observations in problems of elastic stability, *Proceedings of the Royal Society of London: Series A* 135 (1932), p. 601
- [10] Hwang S.F., Mao C.P.: Failure of delaminated interply hybrid composite plates under compression, *Composites Science and Technology* 61 (2001), p. 1513
- [11] Hull D., Shi Y.B.: Damage mechanism characterization in composite damage tolerance investigations, *Composite Structures* 23 (1993), p. 99
- [12] Kumar P., Rai B.: Delaminations of barely visible impact damage in CFRP laminates, *Composite Structures* 23 (1993), p. 313
- [13] Fuoss E., Straznický P.V., Poon C.: Effects of stacking sequence on the impact resistance in composite laminates – part 1: Parametric study, *Composite Structures* 41 (1998), p. 67
- [14] Davies G.A.O., Zhang X.: Predicting impact damage of composite stiffened panels, *The Aeronautical Journal* 104 (2000), p. 97
- [15] Herszberg I., Weller T.: Impact damage resistance of buckled carbon/epoxy panels, *Composite Structures* 73 (2006), p. 130
- [16] Davidson B.D., Gharibian S.J., Yu L.: Evaluation of energy release rate-based approaches for predicting delamination growth in laminated composites, *International Journal of Fracture* 105 (2000), p. 343
- [17] Tay T.E.: Characterization and analysis of delamination fracture in composites: An overview of developments from 1990 to 2001, *Applied Mechanics Reviews* 56 (2003), p. 1
- [18] Pereira A.B., de Moraes A.B.: Mixed-mode I+III interlaminar fracture of carbon/epoxy laminates, *Composites: Part A* 40 (2009), p. 518
- [19] Mathews M.J., Swanson S.R.: Characterization of the interlaminar fracture toughness of a laminated carbon/epoxy composite, *Composites Science and Technology* 67 (2007), p. 1489
- [20] Rikards R.: Interlaminar fracture behaviour of laminated composites, *Computers and Structures* 76 (2000), p. 11
- [21] Sham M.L., Kim J.K., Wu J.S.: Interlaminar properties of glass woven fabric composites: mode I and mode II fracture, *Key Engineering Materials* 145–149 (1998), p. 799
- [22] Singh S., Partridge I.K.: Mixed-mode fracture in an interleaved carbon-fibre/epoxy composite, *Composites Science and Technology* 55 (1995), p. 319
- [23] Szekrényes A.: Delamination fracture analysis in the G_{II} – G_{III} plane using prestressed transparent composite beams, *International Journal of Solids and Structures* 44 (2007), p. 3359
- [24] Nilsson K.F., Storåkers B.: On the interface crack growth in composite plates, *Journal of Applied Mechanics* 59 (1992), p. 530
- [25] Krüger R., Hänsel C., König M.: Experimental-numerical investigation of delamination buckling and growth, Tech. rep. ISD-Report 96/3, Institut für Statik und Dynamik der Luft- und Raumfahrtkonstruktionen, Universität Stuttgart, November 1996

- [26] Anderson J., König M.: Dependence of fracture toughness of composite laminates on interface ply orientations and delamination growth directions, *Composites Science and Technology* 64 (2004), p. 2139
- [27] Kim H.S., Chattopadhyay A., Ghoshal A.: Dynamic analysis of cross-ply composite laminates with embedded multiple delaminations, In: 44th AIAA/ASME/ASCE/AHS/ASC Structures, Structural Dynamics, and Materials Conference, AIAA Inc., 2003, p. 622

Received in editor's office:

Approved for publishing: